Enhanced sensitivity of an all-dielectric refractive index sensor with an optical bound state in the continuum

Dmitrii N. Maksimov,[1,2] Valery S. Gerasimov,[1,3] Andrey A. Bogdanov,[4] and Sergey P. Polyutov[1]
[1]*IRC SQC, Siberian Federal University, 660041, Krasnoyarsk, Russia*
[2]*Kirensky Institute of Physics, Federal Research Center KSC SB RAS, 660036, Krasnoyarsk, Russia*
[3]*Institute of Computational Modeling SB RAS, Krasnoyarsk, 660036, Russia*
[4]*Department of Physics and Engineering, ITMO University, 191002, St. Petersburg, Russia*

(Received 31 January 2022; accepted 9 March 2022; published 23 March 2022)

The sensitivity of a refractive index sensor based on an optical bound state in the continuum is considered. Applying Zel'dovich perturbation theory we derived an analytic expression for bulk sensitivity of an all-dielectric sensor utilizing symmetry protected in-Γ optical bound states in a dielectric grating. The upper sensitivity limit is obtained. A recipe is proposed for obtaining the upper sensitivity limit by optimizing the design of the grating. It is shown that the maximal sensitivity can be achieved regardless to the permittivity of the constituent dielectric of the system. The results are confirmed through direct numerical simulations.

DOI: 10.1103/PhysRevA.105.033518

I. INTRODUCTION

Recently, we have witnessed a surge of interest to bound states in the continuum (BICs) [1–3] that have revolutionized nanophotonics by paving a way to high throughput optical sensing devices with enhanced light-matter interaction at the nanoscale [4–11]. The most remarkable feature of BICs is the occurrence of high-quality Fano resonances in the transmittance spectrum [12–15]. The Fano resonances emerge when the system's symmetry is broken, so the otherwise localized BIC mode can couple with impinging light [16,17]. The spectral position of these extremely narrow Fano resonances is affected by the refractive index of the surrounding medium allowing to design optical sensors with an excellent figure of merit (FOM) [18–23] as the narrow Fano feature can be easily resolved in the spectral measurements. Despite the unsurpassed FOM, the major drawback of the dielectric sensors in comparison against the plasmonic ones is a noticeably (approximately five times) less sensitivity [24]. Nowadays, comparative analysis of dielectric sensors performance is already available in the existing literature [25,26]. Yet, to the best of our knowledge, there is no exhaustive theory providing a clear optimization procedure that would lead to the maximal sensitivity of a BIC sensor. In our previous paper [17] we argued that the maximal sensitivity of a BIC sensor is given by $S_{\max} = \lambda_{\mathrm{BIC}}/n_c$, where λ_{BIC} is the vacuum wavelength of the BIC, and n_c is the cladding fluid refractive index, i.e., the physical quantity whose variation is measured by the sensor.

In this paper, we provide a route for achieving the maximal bulk refractive index sensitivity by considering optical BICs whose spectral position approaches the diffraction threshold. An analytic expression for a BIC vacuum wavelength shift is derived by applying the Zel'dovich perturbation theory [27]. The primary advantage of the Zel'dovich approach is that it can be applied to optical delocalized eigenmodes [28] to have already been proved useful in theory of plasmonic sensors [29]. The onset of diffraction usually has a negative impact on high-Q resonances, particularly on BICs which are typically destroyed by the radiation losses [30]. However, in the situation when the first-order diffraction cutoff frequency is not yet exceeded the evanescent field are demonstrated to provide the largest overlap with the cladding fluid leading to enhanced sensitivity [31].

II. THE SYSTEM

One of the most important platforms for implementing optical BICs is subwavelength dielectric gratings [30,32–39] which have been extensively studied for sensing applications with both dielectric [17,40–43] and plasmonic structures [44]. The system under consideration is a subwavelength dielectric grating of period $h = 300$ nm made of TiO_2 bars with width $w = 0.5h$. In our numerical simulations, we use $n_g = 2.485$ as the refractive index of the grating while the material losses are ignored so the absorption coefficient is set to zero. The TiO_2 grating is placed on top of a glass substrate with refractive index $n_s = 1.5$ as shown in Fig. 1(a). The geometric parameters of the grating are specified in the caption to Fig. 1. The propagation of TE modes is controlled by the Helmholtz equation

$$\nabla^2 E_x(y,z) + k^2 \epsilon(y,z) E_x(y,z) = 0, \tag{1}$$

where E_x is the x component of the electric field, $\epsilon = f(y,z)$ is the coordinate-dependant dielectric function, ∇^2 is the two-dimensional (2D) Laplacian operator, and $k = \omega/c$ is the vacuum wave number. The spectrum of the diffraction channels into to the cladding fluid is given by

$$(n_c k)^2 = \left(\beta + \frac{2\pi m}{h}\right)^2 + k_z^2, \tag{2}$$

where m is an integer, k_z is the z component of the outgoing wave vector, β is the propagation constant with respect to the

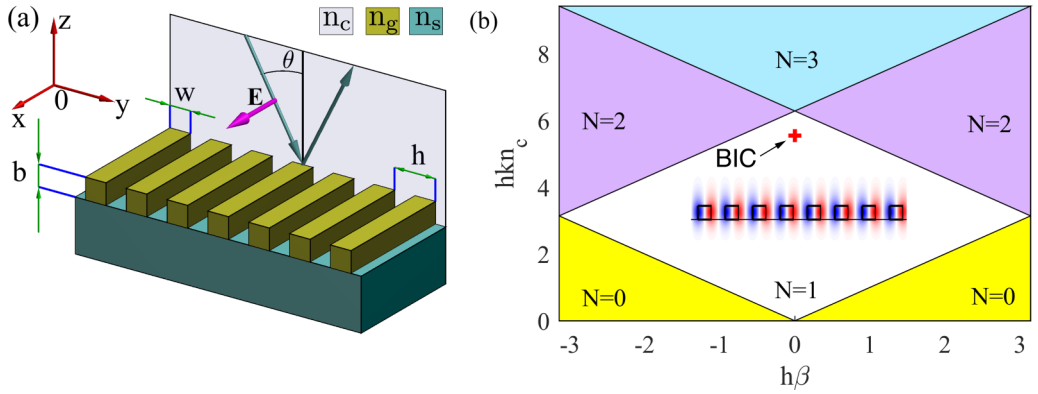

FIG. 1. BIC in dielectric grating. (a) TiO_2 dielectric grating on a glass substrate, $h = 300$ nm, $b = 0.5h$, $w = 0.5h$, $n_g = 2.485$, and $n_s = 1.5$. The magenta arrow is the electric vector of an incident s wave. (b) Number of scattering channels allowed for diffraction. The red star indicates the position of a symmetry protected BIC with $hk_{\mathrm{BIC}}n_c = 3.262$, $n_c = 1.7$. The BIC mode profile is depicted below its spectral position in procedure defined units with red areas corresponding to positive E_x whereas in the blue areas E_x is negative.

y axis, and n_c is the refractive index of the cladding fluid. All simulation results referenced throughout the paper have been obtained with application of the FDTD Lumerical photonics simulation software solution [45].

Following our previous work [17], we consider a symmetry protected in-Γ BIC which does not radiate to the far field because it is symmetrically mismatched with the zeroth-order diffraction channel. In engineering, a symmetry protected BIC it is of key importance to ensure that the higher diffraction orders are not allowed at the BIC wavelength. Once diffraction is allowed either in the substrate or in the superstrate (cladding fluid), the BIC is destroyed being transformed into a leaky mode radiating into the diffraction channels [30]. The positions of the frequency cutoffs are given by the following equations:

$$n_c k = |\beta|, \quad n_c k = \beta + \frac{2\pi m}{h} \quad \text{if } m > 0,$$
$$n_c k = -\beta - \frac{2\pi m}{h} \quad \text{if } m < 0. \tag{3}$$

In Fig. 1(b), we demonstrate the number of diffraction channels N allowed in the cladding depending on the spectral parameters of the incident wave, namely, its vacuum wave number, k and the propagation constant in the y direction β. Each colored domain in Fig. 1(b) corresponds to the specified value of N. The symmetry protected in-Γ BIC is destroyed due to opening diffraction channels with $m = \pm 1$ when $hk_{\mathrm{BIC}}n_c > 2\pi$. For the considered structure BIC lies in the domain of the specular reflection where only the zero-order diffraction channel ($m = 0$) is open. The frequency of BIC is shown by a red cross in Fig. 1(b). The BIC field profile is shown in the inset. It is important for our future analysis to point out that the BIC mode profile has the following asymptotic far-field expression

$$E_x \propto e^{-\varkappa z} \sin\left(\frac{2\pi y}{h}\right), \tag{4}$$

where

$$\varkappa = \sqrt{\left(\frac{2\pi}{h}\right)^2 - \epsilon_\infty^{(0)} k^2}, \tag{5}$$

with $\epsilon_\infty^{(0)} = n_c^2$ and $y = 0$ corresponding to the geometric center of the unit cell. Notice that in Eq. (4) we only retained the contribution of the first-order evanescent diffraction channels, since the higher-order channels decay much faster with the increase of z.

III. PERTURBATION THEORY

The Zel'dovich [27] perturbation approach is introduced by writing a series expansion in the increment of the dielectric function $\Delta\epsilon$,

$$\epsilon = \epsilon^{(0)} + \Delta\epsilon, \quad k = k^{(0)} + \Delta k, \quad E_x = E_x^{(0)} + E_x^{(1)}. \tag{6}$$

By definition the function $\epsilon^{(0)}$ is the total coordinate-dependent dielectric function with the reference value of the cladding fluid refractive index, whereas $\Delta\epsilon$ is the increment of the dielectric constant of the cladding fluid. Substituting the above expansions into Eq. (1) we have up to the first perturbation order

$$\nabla^2 E_x^{(0)} + \epsilon^{(0)}(k^{(0)})^2 E_x^{(0)} = 0, \tag{7}$$

$$\nabla^2 E_x^{(1)} + \epsilon^{(0)}(k^{(0)})^2 E_x^{(1)} = -\Delta\epsilon(k^{(0)})^2 E_x^{(0)} - 2\epsilon^{(0)}\Delta k k^{(0)} E_x^{(0)}. \tag{8}$$

Following Zel'dovich we multiply Eq. (8) by $E_x^{(0)}$ and integrate within the limits specified below

$$\int_{-h/2}^{h/2} dy \int_{-d}^{d} dz E_x^{(0)}\left[\nabla^2 E_x^{(1)} + \epsilon^{(0)}(k^{(0)})^2 E_x^{(1)}\right] = -\int_{-h/2}^{h/2} dy \int_{-d}^{d} dz\left[\Delta\epsilon(k^{(0)})^2 + 2\epsilon^{(0)}\Delta k k^{(0)}\right]\left(E_x^{(0)}\right)^2, \tag{9}$$

where $d > b$ is an arbitrary distance from the grating. By applying Green's theorem together with Eq. (7) one rewrites the left-hand side of Eq. (9) in the following manner:

$$\int_{-h/2}^{h/2} dy \int_{-d}^{d} dz E_x^{(0)}\left[\nabla^2 E_x^{(1)} + \epsilon^{(0)}(k^{(0)})^2 E_x^{(1)}\right] = \int_{\ell} d\ell\left(E_x^{(0)}\frac{\partial E_x^{(1)}}{\partial n} - E_x^{(1)}\frac{\partial E_x^{(0)}}{\partial n}\right), \tag{10}$$

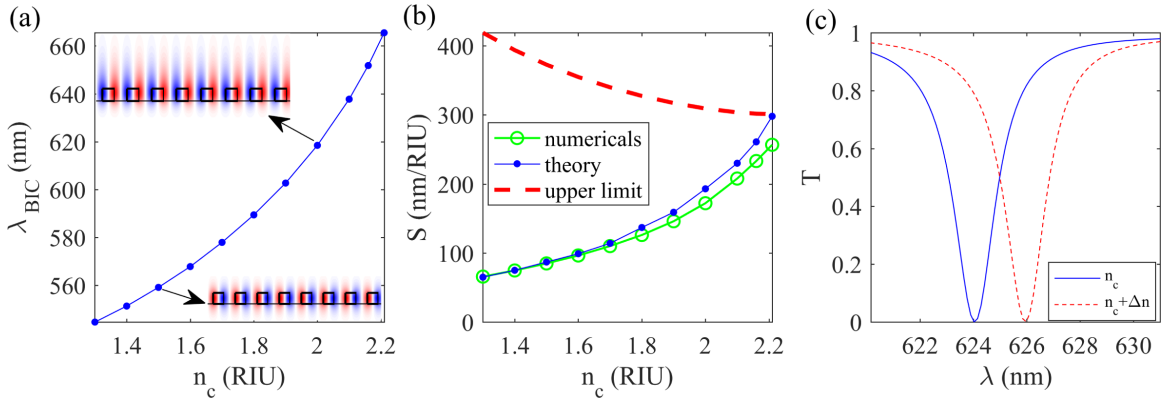

FIG. 2. Fano resonance shift and differential sensitivity. (a) The vacuum wavelength of the symmetry protected BIC as a function of the cladding fluid refractive index. (b) Differential sensitivity obtained from Eq. (15)—circles, and through the shift of the Fano resonance—dots at $\theta = 2^\circ$. The dash line shown the upper limit of sensitivity Eq. (16). (c) Shift of the Fano resonance obtained at $\theta = 2^\circ$, $n_c = 2.0$ with $\Delta n = 0.01$.

where ℓ is a path encircling the integration domain of the left-hand side in the clockwise direction. The integrals along the lines $y = -h/2$ and $y = h/2$ cancel each other due to periodicity while the integral along $z = -d$ can be neglected because we assume that the BIC field decays faster in the substrate because of a lesser refractive index. This leads us to

$$\int_{-h/2}^{h/2} dy \int_{-d}^{d} dz E_x^{(0)} \left[\nabla^2 E_x^{(1)} + \epsilon^{(0)} (k^{(0)})^2 E_x^{(1)}\right] = \int_{-h/2}^{h/2} dy \left(E_x^{(0)} \frac{\partial E_x^{(1)}}{\partial z} - E_x^{(1)} \frac{\partial E_x^{(0)}}{\partial z} \right)\Big|_{z=d}. \tag{11}$$

Equating the right-hand side of Eq. (11) to that of Eq. (9) and inserting the following asymptotic expressions:

$$\frac{\partial E_x^{(0)}}{\partial z} = -\varkappa^{(0)} E_x^{(0)},$$
$$\frac{\partial E_x^{(1)}}{\partial z} = \frac{1}{2\varkappa^{(0)}} \left[\Delta\epsilon (k^{(0)})^2 + 2\epsilon_\infty^{(0)} k^{(0)} \Delta k\right] E_x^{(0)} - \varkappa^{(0)} E_x^{(1)}, \tag{12}$$

one has

$$\frac{\Delta k}{\Delta \epsilon} = -\frac{k^{(0)}}{2} I, \tag{13}$$

where

$$I = \frac{\int_{S_c} dS (E_x^{(0)})^2 + \frac{1}{2\varkappa^{(0)}} \int_{-h/2}^{h/2} dy [E_x^{(0)}(y,d)]^2}{\int_{S_{\text{tot}}} dS \epsilon^{(0)} \left(E_x^{(0)}\right)^2 + \frac{\epsilon_\infty^{(0)}}{2\varkappa^{(0)}} \int_{-h/2}^{h/2} dy \left[E_x^{(0)}(y,d)\right]^2}. \tag{14}$$

Thus, for the differential sensitivity $S = \Delta\lambda_{\text{BIC}}/\Delta n_c$ we have

$$S = \lambda n_c I. \tag{15}$$

On approach to the cutoff of the first-order diffraction channels $\varkappa \to 0$ we have

$$S = \frac{\lambda_{\text{BIC}}}{n_c}, \tag{16}$$

which coincides with the upper sensitivity limit predicted in Ref. [17]. Before proceeding to numerical validation of the newfound results some comments are due on the choice of d. It is obvious that d should be taken large enough to guarantee that the far-field asymptotic behavior be given by Eq. (4). In the domain of specular reflection at the normal incidence the evanescent fields of the second-order diffraction channels decay faster than $e^{-2\pi z/h}$. Therefore, for a practical choice it is sufficient to take $d > \lambda_{\text{BIC}}$. At the save time, from the computation viewpoint the choice of d determines the size of the computational domain. Technically, d is the distance at which the PML absorbers are placed to set up reflectionless boundary conditions. Thus, application of Eqs. (14) and (15) allows us to predict the sensitivity of BICs with the evanescent fields extended beyond the computational domain.

IV. NUMERICAL VALIDATION

In Fig. 2(a) we plotted the vacuum wavelength of the symmetry protected BIC at different values of n_c. One can see from Fig. 2(a) that λ_{BIC} decreases with the increase of n_c especially at larger values of n_c. In Fig. 2(b) we plotted the values of differential sensitivity obtained by two different methods. The "theoretical" result is obtained by directly applying Eq. (15) meanwhile the "numerical" values are obtained finding the shift of a BIC-induced Fano resonance under illumination by a plane wave at the incidence angle $\theta = 2^\circ$. To keep the approach consistent while changing n_c, the incidence angle θ is defined in reference to the wave vectors in the outer space (air), so the incident angle within the cladding fluid θ_c is found through the formula

$$n_c \sin(\theta_c) = \sin(\theta). \tag{17}$$

The typical picture of the shift in the resonance position is shown in Fig. 2(c). In Fig. 2(b) we also plotted the maximal value of the sensitivity according to Eq. (16). One can see from Fig. 2(b) that with the increase of n_c, the sensitivity approaches the upper limit given by Eq. (16). Notice that, at larger n_c, the numerically observed sensitivity deviates from the theoretical expressions [(14), (15)]. This is because the first-order frequency cutoffs are lower at $\theta \neq 0^\circ$ according to Eq. (3), see also Fig. 2(b). In our case, the onset of diffraction at $n_c = 2.21$ destroys the high-Q resonance with the chosen angle of incidence $\theta = 2^\circ$ although the BIC proper is not

yet destroyed. Finally, notice that the observed sensitivity enhancement can be easily understood from Fig. 2(a) which is complemented with subplots of two BIC profiles. One can see that, at larger n_c, the BIC fields are further extended into the upper half-space providing a better overlap with the cladding fluid.

V. CONCLUSION

In this paper, we have demonstrated an approach allowing to achieve the upper sensitivity limit for an all-dielectric sensor based on an optical bound state in the continuum (BIC). The analytic expressions for computing the bulk sensitivity from the BIC vacuum wavelength and mode profile have been derived as Eqs. (14), and (15). The most remarkable feature of the obtained expressions is that the maximal sensitivity is independent of the material and geometric parameters of the grating once the BIC approaches the first diffraction order threshold. This feature allows for freedom in choosing of the constituent dielectric. All that is necessary for achieving the maximal sensitivity is to vary the geometric parameters for the BIC eigenfrequency approaching the cutoffs of the first-order diffraction channels. The BICs are topologically protected objects [8,46,47] and, therefore, they are not destroyed under variation of geometric parameters complying with the structure point-group symmetry as far as the BIC eigenfrequency remains in the spectral domain of the specular reflection [34]. In the regime of the maximal sensitivity the vacuum wavelength of the in-Γ BIC is always given by

$$\lambda_{\mathrm{BIC}} = n_c h, \tag{18}$$

while the maximal sensitivity is simply $S_{\max} = \lambda_{\mathrm{BIC}}/n_c$. Notice that, due to the scaling invariance of Maxwell's equations, λ_{BIC} can be tuned to any desired wavelength by isometric transformation of the grating.

In the numerical example proposed, the maximal sensitivity has been achieved with a relatively large value of the cladding fluid refractive index $n_c = 2.21$. This, of course, out of the range required in practical applications which are stuck around the refractive index of water. Importantly, achieving the maximal sensitivity requires the refractive index of the cladding larger than that of substrate. If the situation is the opposite, the first-order diffraction channels will first open in the substrate [30] destroying the BIC before the maximal overlap with the cladding has been achieved. There are two possible solutions to this problem. The first is, obviously, applying a low index substrate [48]. The second is using a substrate of a properly chosen Bragg reflector [49] which would isolate the lower half-space by a photonic band gap for the outgoing waves of the first order of diffraction. This problem will be addressed in the future studies.

ACKNOWLEDGMENTS

The theoretical part of the research was supported by the Ministry of Science and High Education of Russian Federation, Project No. FSRZ-2020-0008, by Russian Foundation for Basic Research, Government of Krasnoyarsk Territory, Krasnoyarsk Regional Fund of Science (Grant No. 20-42-240003). The numerical part is supported by the Russian Science Foundation (21-72-30018).

[1] C. W. Hsu, B. Zhen, A. D. Stone, J. D. Joannopoulos, and M. Soljačić, Bound states in the continuum, Nat. Rev. Mater. **1**, 16048 (2016).

[2] K. Koshelev, G. Favraud, A. Bogdanov, Y. Kivshar, and A. Fratalocchi, Nonradiating photonics with resonant dielectric nanostructures, Nanophotonics **8**, 725 (2019).

[3] A. F. Sadreev, Interference traps waves in open system: Bound states in the continuum, Rep. Prog. Phys. **84**, 055901 (2021).

[4] M. I. Molina, A. E. Miroshnichenko, and Y. S. Kivshar, Surface Bound States in the Continuum, Phys. Rev. Lett. **108**, 070401 (2012).

[5] S. Romano, G. Zito, S. Managò, G. Calafiore, E. Penzo, S. Cabrini, A. C. D. Luca, and V. Mocella, Surface-enhanced Raman and fluorescence spectroscopy with an all-dielectric metasurface, J. Phys. Chem. C **122**, 19738 (2018).

[6] E. N. Bulgakov and A. F. Sadreev, Bound states in the continuum in photonic waveguides inspired by defects, Phys. Rev. B **78**, 075105 (2008).

[7] E. Penzo, S. Romano, Y. Wang, S. Dhuey, L. Dal Negro, V. Mocella, and S. Cabrini, Patterning of electrically tunable light-emitting photonic structures demonstrating bound states in the continuum, J. Vac. Sci. Technol. B **35**, 06G401 (2017).

[8] B. Zhen, C. W. Hsu, L. Lu, A. Douglas Stone, and M. Soljačić, Topological Nature of Optical Bound States in the Continuum, Phys. Rev. Lett. **113**, 257401 (2014).

[9] V. Mocella and S. Romano, Giant field enhancement in photonic resonant lattices, Phys. Rev. B **92**, 155117 (2015).

[10] K. Koshelev, A. Bogdanov, and Y. Kivshar, Meta-optics and bound states in the continuum, Sci. Bull. **64**, 836 (2019).

[11] G. Zito, S. Romano, S. Cabrini, G. Calafiore, A. C. De Luca, E. Penzo, and V. Mocella, Observation of spin-polarized directive coupling of light at bound states in the continuum, Optica **6**, 1305 (2019).

[12] S. P. Shipman and S. Venakides, Resonant transmission near nonrobust periodic slab modes, Phys. Rev. E **71**, 026611 (2005).

[13] A. F. Sadreev, E. N. Bulgakov, and I. Rotter, Bound states in the continuum in open quantum billiards with a variable shape, Phys. Rev. B **73**, 235342 (2006).

[14] Cédric Blanchard, Jean-Paul Hugonin, and C. Sauvan, Fano resonances in photonic crystal slabs near optical bound states in the continuum, Phys. Rev. B **94**, 155303 (2016).

[15] E. N. Bulgakov and D. N. Maksimov, Optical response induced by bound states in the continuum in arrays of dielectric spheres, J. Opt. Soc. Am. B **35**, 2443 (2018).

[16] K. Koshelev, S. Lepeshov, M. Liu, A. Bogdanov, and Y. Kivshar, Asymmetric Metasurfaces with High-Q Resonances Governed by Bound States in the Continuum, Phys. Rev. Lett. **121**, 193903 (2018).

[17] D. N. Maksimov, V. S. Gerasimov, S. Romano, and S. P. Polyutov, Refractive index sensing with optical bound states in the continuum, Opt. Express **28**, 38907 (2020).

[18] Y. Liu, W. Zhou, and Y. Sun, Optical refractive index sensing based on high-Q bound states in the continuum in free-space coupled photonic crystal slabs, Sensors **17**, 1861 (2017).

[19] S. Romano, G. Zito, S. Torino, G. Calafiore, E. Penzo, G. Coppola, S. Cabrini, I. Rendina, and V. Mocella, Label-free sensing of ultralow-weight molecules with all-dielectric metasurfaces supporting bound states in the continuum, Photonics Res. **6**, 726 (2018).

[20] S. Romano, A. Lamberti, M. Masullo, E. Penzo, S. Cabrini, I. Rendina, and V. Mocella, Optical biosensors based on photonic crystals supporting bound states in the continuum, Materials **11**, 526 (2018).

[21] F. Yesilkoy, E. R. Arvelo, Y. Jahani, M. Liu, A. Tittl, V. Cevher, Y. Kivshar, and H. Altug, Ultrasensitive hyperspectral imaging and biodetection enabled by dielectric metasurfaces, Nat. Photonics **13**, 390 (2019).

[22] S. Mukherjee, J. Gomis-Bresco, P. Pujol-Closa, D. Artigas, and L. Torner, Angular control of anisotropy-induced bound states in the continuum, Opt. Lett. **44**, 5362 (2019).

[23] H. Vyas and R. S. Hegde, Improved refractive-index sensing performance in medium contrast gratings by asymmetry engineering, Opt. Mater. Express **10**, 1616 (2020).

[24] N. Bosio, H. Šípová-Jungová, N. O. Länk, T. J. Antosiewicz, R. Verre, and M. Käll, Plasmonic versus all-dielectric nanoantennas for refractometric sensing: A direct comparison, ACS Photonics **6**, 1556 (2019).

[25] G. Pitruzzello and T. F. Krauss, Photonic crystal resonances for sensing and imaging, J. Opt. (Bristol, U. K.) **20**, 073004 (2018).

[26] J. Wang, J. Yang, H. Zhao, and M. Chen, Quasi-BIC-governed light absorption of monolayer transition-metal dichalcogenide-based absorber and its sensing performance, J. Phys. D: Appl. Phys. **54**, 485106 (2021).

[27] Ya B. Zel'dovich, On the theory of unstable states, Sov. Phys. JETP **12**, 542 (1961).

[28] H. M. Lai, P. T. Leung, K. Young, P. W. Barber, and S. C. Hill, Time-independent perturbation for leaking electromagnetic modes in open systems with application to resonances in microdroplets, Phys. Rev. A **41**, 5187 (1990).

[29] S. J. Zalyubovskiy, M. Bogdanova, A. Deinega, Y. Lozovik, A. D. Pris, K. H. An, W. Paige Hall, and R. A. Potyrailo, Theoretical limit of localized surface plasmon resonance sensitivity to local refractive index change and its comparison to conventional surface plasmon resonance sensor, J. Opt. Soc. Am. A **29**, 994 (2012).

[30] Z. F. Sadrieva, I. S. Sinev, K. L. Koshelev, A. Samusev, I. V. Iorsh, O. Takayama, R. Malureanu, A. A. Bogdanov, and A. V. Lavrinenko, Transition from optical bound states in the continuum to leaky resonances: Role of substrate and roughness, ACS Photonics **4**, 723 (2017).

[31] S. Romano, G. Zito, Sofía N. Lara Yépez, S. Cabrini, E. Penzo, G. Coppola, I. Rendina, and V. Mocellaa, Tuning the exponential sensitivity of a bound-state-in-continuum optical sensor, Opt. Express **27**, 18776 (2019).

[32] D. C. Marinica, A. G. Borisov, and S. V. Shabanov, Bound States in the Continuum in Photonics, Phys. Rev. Lett. **100**, 183902 (2008).

[33] F. Monticone and A. Alù, Bound states within the radiation continuum in diffraction gratings and the role of leaky modes, New J. Phys. **19**, 093011 (2017).

[34] E. N. Bulgakov, D. N. Maksimov, P. N. Semina, and S. A. Skorobogatov, Propagating bound states in the continuum in dielectric gratings, J. Opt. Soc. Am. B **35**, 1218 (2018).

[35] E. N. Bulgakov and D. N. Maksimov, Avoided crossings and bound states in the continuum in low-contrast dielectric gratings, Phys. Rev. A **98**, 053840 (2018).

[36] Sun-Goo Lee and R. Magnusson, Band dynamics of leaky-mode photonic lattices, Opt. Express **27**, 18180 (2019).

[37] D. A. Bykov, E. A. Bezus, and L. L. Doskolovich, Coupled-wave formalism for bound states in the continuum in guided-mode resonant gratings, Phys. Rev. A **99**, 063805 (2019).

[38] X. Gao, B. Zhen, M. Soljačić, H. Chen, and C. W. Hsu, Bound states in the continuum in fiber Bragg gratings, ACS Photonics **6**, 2996 (2019).

[39] H. Hemmati and R. Magnusson, Resonant dual-grating metamembranes supporting spectrally narrow bound states in the continuum, Adv. Opt. Mater. **7**, 1900754 (2019).

[40] H. Zhang, T. Wang, J. Tian, J. Sun, S. Li, I. De Leon, R. P. Zaccaria, L. Peng, F. Gao, X. Lin, H. Chen, and G. Wang, Quasi-BIC laser enabled by high-contrast grating resonator for gas detection, Nanophotonics **11**, 297 (2022).

[41] G. Finco, M. Z. Bideskan, L. Vertchenko, L. Y. Beliaev, R. Malureanu, L. R. Lindvold, O. Takayama, P. E. Andersen, and A. V. Lavrinenko, Guided-mode resonance on pedestal and half-buried high-contrast gratings for biosensing applications, Nanophotonics **10**, 4289 (2021).

[42] G. C. Park and K. Park, Critically coupled Fabry-Perot cavity with high signal contrast for refractive index sensing, Sci. Rep. **11**, 19575 (2021).

[43] S. Mesli, H. Yala, M. Hamidi, A. BelKhir, and F. I. Baida, High performance for refractive index sensors via symmetry-protected guided mode resonance, Opt. Express **29**, 21199 (2021).

[44] S. Jia, Z. Li, and J. Chen, High-sensitivity plasmonic sensor by narrowing Fano resonances in a tilted metallic nano-groove array, Opt. Express **29**, 21358 (2021).

[45] Lumerical FDTD Solutions, https://www.lumerical.com.

[46] E. N. Bulgakov and D. N. Maksimov, Topological Bound States in the Continuum in Arrays of Dielectric Spheres, Phys. Rev. Lett. **118**, 267401 (2017).

[47] E. N. Bulgakov and D. N. Maksimov, Bound states in the continuum and polarization singularities in periodic arrays of dielectric rods, Phys. Rev. A **96**, 063833 (2017).

[48] E. F. Schubert, J. K. Kim, and J.-Q. Xi, Low-refractive-index materials: A new class of optical thin-film materials, Phys. Status Solidi B **244**, 3002 (2007).

[49] R. G. Bikbaev, D. N. Maksimov, P. S. Pankin, K.-P. Chen, and I. V. Timofeev, Critical coupling vortex with grating-induced high q-factor optical Tamm states, Opt. Express **29**, 4672 (2021).